Elastic electron backscattering from surfaces: Prediction of maximum intensity

A. Jablonski
Institute of Physical Chemistry, Polish Academy of Sciences, ulica Kasprzaka 44/52, 01-224 Warszawa, Poland

C. Jansson and S. Tougaard
Fysisk Institut, Odense Universitet, Campusvej 55, DK-5230 Odense M, Denmark
(Received 7 August 1992)

In the present work, systematic Monte Carlo simulations were applied to calculate the intensity of elastically backscattered electrons as a function of energy and exit angle for 27 elements in the energy range from 50 to 2000 eV. By comparison to available experimental data, it is found that the applied theory accounts well for the shape of the energy dependence as well as for the absolute values of the elastic reflection coefficient. As a function of energy, the intensity of elastically backscattered electrons is usually found to pass a maximum. For each element, the energy position of this maximum and the corresponding intensity has been determined as a function of the direction with respect to the surface normal. It is found that the results for all 27 elements can be summarized by division into five characteristic groups corresponding to a different number of maxima or to distinctly different intensities. These groups can be defined by separate ranges of the atomic number. Representative results for each of these five groups are shown in detail. Knowledge of the position of the maximum and its value may be important to optimize such experimental surface-sensitive techniques that make use of elastically backscattered electrons in the energy range 50–3000 eV.

I. INTRODUCTION

The effect of elastic electron backscattering from surfaces plays an important role in a number of experimental techniques. Elastic backscattering from surfaces of single crystals is a basis of low-energy electron diffraction (LEED). The phenomenon of elastic backscattering contributes to the signals of disappearance-potential spectroscopy (DAPS) (Refs. 1 and 2) and high-energy appearance-potential spectroscopy (HEAPS).[3] Furthermore, maximization of the elastic peak intensity is a standard procedure for bringing the sample to the focus of the cylindrical mirror analyzer (CMA). The acronym EPES (elastic peak electron spectroscopy) has been proposed for the experimental techniques which relate the effect of elastic backscattering with the surface properties of the studied solid.[4–10] A very useful application of this technique is determination of the inelastic mean free path (IMFP) of electrons in solids from the measured intensity of the elastic peak.[11–13] Use of the elastically backscattered electrons in scanning electron microscopy (SEM) has important advantages. Schmid, Gaukler, and Seiler[14] have shown that the contrast in SEM images produced by elastically reflected electrons is better, by more than one order of magnitude, than the contrast achieved with backscattered electrons. Moreover, smaller depth of analysis by SEM and better resolution is obtained with elastically reflected electrons or electrons with small energy loss.[15]

The effect of elastic backscattering is usually described by two parameters:

(1) The reflection coefficient, which is the probability that an electron of the incident beam will leave the solid without energy loss; this parameter, for practical reasons, is usually measured within a certain solid angle.

(2) The angular distribution of the elastically backscattered electrons.

These parameters were determined experimentally in numerous studies made for different polycrystalline solids and energies.[4,7–10,14,16–24] The elastic backscattering probability is related to the elastic scattering cross sections corresponding to the scattering centers of a given solid. Since the total elastic scattering cross section always decreases monotonically with energy,[25] one would expect that the reflection coefficient should diminish with energy increase. However, Bronshtein and Pronin[20] and Schmid, Gaukler, and Seiler,[14] who both provide very extensive experimental material, have shown that a maximum exists in the energy dependences of the elastically backscattered current. The position of this maximum depends on the atomic number of the target material. Similar observations were made by other authors.[7–10,22] The existence of this maximum was also confirmed by theory.[26,27] It seems to be due to a complex structure of the differential elastic scattering cross sections in the considered energy range (50–3000 eV). The general information on the energy position of the maximum intensity of elastically backscattered electrons may be useful for the experimental techniques which rely on the phenomenon of elastic backscattering. The objective of the present work is then to analyze the behavior of the energy dependence of the reflection coefficient for a wide range of atomic numbers and for different experimental geometries.

II. THEORY

Generally, the theoretical model of the electron transport in solids may be formulated analytically or may be

described by the Monte Carlo model. In the analytical models, simplifying assumptions concerning the process of multiple elastic collisions are necessary. These simplifications are not needed in the Monte Carlo approach, for which reason it does provide a more realistic and accurate description of elastic backscattering from surfaces.[26] Actually, any theoretical model describing the electron transport is based on a number of assumptions specifying the structure of the solid and the interaction of an electron with the solid. The following three assumptions are usually made:

(1) A given solid is a set of randomly distributed scattering centers corresponding to atoms constituting the considered solid.

(2) The high-energy electron is interacting with only one scattering center during the scattering event. Potentials of other centers are neglected.

(3) Each considered scattering center of a solid is approximated by the potential of the corresponding isolated atom.

The theory of elastic backscattering from surfaces presented here was very successfully used to explain experimental observations made in a wide range of energies, solids, and for numerous experimental geometries.[24,26,27] This theory will be briefly recapitulated in the following sections.

A. Elastic scattering of electrons: Nonrelativistic approach

In view of the above assumptions, an accurate description of the two-body interaction, electron-scattering center, is required in any theoretical model of electron transport. Elastic collision of an electron with an atom is a well-known problem in quantum mechanics.[28–30] Tedious calculations are usually associated with the solution of this problem, and in practice a number of additional assumptions are made to simplify the numerical procedure. Unfortunately, in the energy range of the surface-sensitive electron spectroscopies (50–3000 eV) the usual simplifying approaches (first-order Born approximation, screened Rutherford cross section), are not valid and the accurate solution of the scattering problem is required.[26]

The interaction between an electron and the central field potential $V(r)$ is described by the Schrödinger equation

$$\left[\Delta+K^2-\frac{2m}{\hbar^2}V(r)\right]\psi(\mathbf{r})=0\ , \tag{1}$$

where K is the length of the wave vector describing the incoming electron and the remaining notation has the usual meaning. At large distances from the scattering center the solution $\psi(\mathbf{r})$ should approach a superposition of the plane incident wave and the outgoing spherical wave

$$\psi(\mathbf{r}) \underset{r\to\infty}{\rightarrow} \exp(i\mathbf{K}\cdot\mathbf{r})+\frac{1}{r}f(\theta)\exp(iKr)\ . \tag{2}$$

The functional dependence on the scattering angle θ is accounted for by the function $f(\theta)$, called the scattering amplitude, which is related to the elastic scattering cross section $d\sigma/d\Omega$:

$$d\sigma/d\Omega=|f(\theta)|^2\ . \tag{3}$$

Thus knowledge of the function $f(\theta)$ is sufficient to determine the differential elastic scattering cross section and, on integration, the total elastic scattering cross section.

The partial-wave expansion method, which is the most general method for solving the scattering problem defined by Eqs. (1)–(3), had been proposed in 1927.[31] It consists in expanding the wave function $\psi(\mathbf{r})$ into the series of the Legendre polynomials since the scattering problem is axially symmetric with respect to the direction of the incoming electron.

$$\psi(\mathbf{r})=\frac{1}{r}\sum_{l=0}^{\infty}A_l u_l(r)P_l(\cos\theta)\ ,$$

where A_l is a constant depending on l, and the functions $u_l(r)$ are solutions of the differential equations

$$\frac{d^2u_l}{dr^2}+\left[K^2-\frac{l(l+1)}{r^2}-\frac{2m}{\hbar^2}V(r)\right]u_l=0\ . \tag{4}$$

The boundary conditions are the following:

$$\begin{aligned} &u_l(0)=0\ ,\\ &u_l(r) \underset{r\to\infty}{\rightarrow} \sin(Kr-l\pi/2+\delta_l)\ , \end{aligned} \tag{5}$$

where δ_l is the so-called phase shift. It is the shift of the function $u_l(r)$ at certain large values of r with respect to the solution of Eq. (4) obtained in the absence of potential, i.e., obtained for $V(r)\equiv 0$. One can prove that the scattering amplitude $f(\theta)$ is expressed in terms of the series of phase shifts δ_l,

$$f(\theta)=\frac{1}{2iK}\sum_{l=0}^{\infty}(2l+1)[\exp(2i\delta_l)-1]P_l(\cos\theta)\ . \tag{6}$$

Calogero[30] proposed the so-called variable phase method for determining the phase shifts. This method involves transformation of the second-order radial Schrödinger equation into the equivalent first-order differential equation. As a result of this transformation one obtains the equation[30]

$$\frac{d\delta_l(r)}{dr}=-\frac{1}{K}\frac{2m}{\hbar^2}V(r)[\hat{j}_l(Kr)\cos\delta_l(r)-\hat{n}_l(Kr)\sin\delta_l(r)]^2\ , \tag{7}$$

with the initial condition

$$\delta_l(0)=0\ , \tag{8}$$

where $\hat{j}_l(x)$ and $\hat{n}_l(x)$ are the Riccati-Bessel functions and $\delta_l(r)$ is the so-called phase function. This function asymptotically approaches the lth phase shift

$$\lim_{r\to\infty}\delta_l(r)=\delta_l\ .$$

Thus integration of Eq. (7) provides a direct relation between the potential $V(r)$ and the phase shift δ_l at

different distances from the nucleus.

The variable phase method was successfully applied in calculations of elastic scattering cross sections for numerous elements and in a wide range of energies.[26,32] This method makes it possible to calculate the phase shifts for the quantum number l reaching 100. Actually, it turned out that this large number of phase shifts may be necessary to calculate the differential elastic scattering cross section from Eqs. (3) and (6) at energies characteristic for the surface-sensitive electron spectroscopies. The variable phase method provides always the absolute values of the phase shifts with good accuracy, even in the case of small values of δ_l. However, the corresponding calculations may require a considerable amount of computer time. This arises from two reasons:

(1) Numerical integration of Eq. (7) requires a large number of steps to maintain a certain reasonable accuracy.

(2) In each step of numerical integration the Riccati-Bessel functions must be determined. This increases considerably the amount of computations.

Thus high-accuracy calculations may become extremely slow. For such cases a much more effective method has been recently proposed.[27]

Let us make the following substitution into the phase equation (7):

$$\tan\delta_l(r)=\frac{\cos[\gamma_l(r)+Kr]\hat{j}_l(Kr)-\sin[\gamma_l(r)+Kr]\hat{j}'_l(Kr)}{\cos[\gamma_l(r)+Kr]\hat{n}_l(Kr)-\sin[\gamma_l(r)+Kr]\hat{n}'_l(Kr)} , \tag{9}$$

where $\gamma_l(r)$ is a new function of the distance r. We obtain a simple first-order differential equation,

$$\frac{d\gamma_l(r)}{dr}=-\frac{1}{K}\left[\frac{l(l+1)}{r^2}+\frac{2m}{\hbar^2}V(r)\right]\sin^2[\gamma_l(r)+Kr] . \tag{10}$$

This equation, as one can see, does not contain the Riccati-Bessel functions. The functions $\gamma_l(r)$ must satisfy the initial conditions

$$\gamma_1(0)=0 ,$$
$$\lim_{r\to 0}\frac{\gamma_l(r)}{r}=\left.\frac{d\gamma_1(r)}{dr}\right|_{r=0}=-Kl/(l+1) . \tag{11}$$

The details concerning integration of Eq. (10) can be found elsewhere.[27]

In the present work the potential $V(r)$ was described by the Thomas-Fermi-Dirac (TFD) potential.[33,34] The simplicity of this potential considerably facilitates the calculations. Nonetheless, this potential leads to a very reliable description of the elastic backscattering effect.[24,26,27]

B. Elastic scattering of electrons: Relativistic approach

The Dirac equation for an electron interacting with the potential $V(r)$ may be also reduced to a first-order differential equation, as shown by Lin, Sherman, and Percus[35] and Bunyan and Schonfelder.[36] This equation describes the functions $\Phi_l^{\pm}(r)$, which are related to the phase shifts. For each quantum number l we have two solutions denoted by plus (spin-up case) and minus (spin-down case) signs:

$$\frac{d\Phi_l^{\pm}(r)}{dr}=\frac{k^{\pm}}{r}\sin[2\Phi_l^{\pm}(r)]+[W-V(r)]-\cos[2\Phi_l^{\pm}(r)] , \tag{12}$$

where W is the total energy and $k=-l-1$ for the spin-up case or $k=l$ for the spin-down case. The system of units is such that energy is measured in units of m_0c^2 and the distance in units of $\hbar/m_0c$. Two phase shifts $\delta_l^{\pm}$ for each l are calculated from

$$\delta_l^{\pm}=\tan^{-1}\frac{Kj_{l+1}(Kr)-j_l(Kr)[(W+1)\tan\Phi_l^{\pm}+(1+l+k^{\pm})/r]}{Kn_{l+1}(Kr)-n_l(Kr)[(W+1)\tan\Phi_l^{\pm}+(1+l+k^{\pm})/r]} , \tag{13}$$

where $K^2=W^2-1$, $j_l(x)$ and $n_l(x)$ are the spherical Bessel functions [note that $xj_l(x)=\hat{j}_l(x)$ and $xn_l(x)=\hat{n}_l(x)$], and

$$\Phi_l^{\pm}=\lim_{r\to\infty}\Phi_l^{\pm}(r) . \tag{14}$$

The initial condition for integration of Eq. (12) is calculated from the series expansion

$$\Phi_l^{\pm}(r)=\Phi_0+\Phi_1 r+\Phi_2 r^2+\Phi_3 r^3+\cdots , \tag{15}$$

with coefficients Φ_0, Φ_1, Φ_2, and Φ_3 derived by Bunyan and Schonfelder.[36]

As in the case of nonrelativistic calculations, the scattering center was approximated in the present work by the Thomas-Fermi-Dirac potential. The same numerical procedure as in Ref. 27 was used for integration of Eqs. (10) and (12). This procedure made it possible in both cases to maintain the accuracy of eight decimal places in the range of integration.

C. Monte Carlo scheme

The electron trajectory in a solid is considered as a "random walk" in which the direction is changed only as a result of the elastic scattering event. To develop the corresponding algorithm, it is sufficient to specify the rule

for calculating the linear lengths between elastic collisions and the distribution of the scattering angles.

Assuming that the electron trajectory is described by the Poisson stochastic process, the linear step lengths Λ follow the exponential distribution. The corresponding proof is quite straightforward.[37] In that case we have

$$f(\Lambda)=(1/\lambda_e)\exp(-\Lambda/\lambda_e)\ , \tag{16}$$

where $f(\Lambda)$ is the probability density function of the step lengths and λ_e is the elastic mean-free path of the electron. The latter parameter may be calculated from the simple expression[38,39]

$$\lambda_e=(N\sigma_t)^{-1}\ , \tag{17}$$

where N is the atomic density of the solid and σ_t is the total elastic scattering cross section.

At the end of the linear part of the trajectory, the elastic scattering event occurs. This event may be described by two angles: (i) the polar scattering angle, i.e., the angle between initial direction and the direction after collision, and (ii) the azimuthal scattering angle, i.e., the angle measured in the plane perpendicular to the initial direction. The polar scattering angles are simulated according to the probability density function given by the equation

$$H(\theta)=\frac{d\sigma/d\theta}{\sigma_t}=\frac{(d\Omega/d\theta)(d\sigma/d\Omega)}{\sigma_t}=\frac{2\pi\sin\theta(d\sigma/d\Omega)}{\sigma_t}\ . \tag{18}$$

This requires knowledge of accurate elastic scattering cross sections. As a consequence of the cylindrical symmetry of the scattering problem, the azimuthal scattering angles are assumed to follow the uniform distribution.

The electron trajectory is followed in the solid until the electron leaves the solid, or until the total trajectory length becomes so large that the contribution to the observed backscattered intensity can be neglected. The contribution from the kth electron to the current collected by the analyzer with the solid angle $\Delta\Omega$ is calculated from

$$\Delta I_k=\begin{cases}\exp(-x_k/\lambda) & \text{if the electron left the solid within acceptance angle of the analyzer}\\ 0 & \text{if the electron did not enter the analyzer}\ ,\end{cases} \tag{19}$$

where λ is the electron inelastic mean free path in the solid, and x_k is the total length traveled by the electron in the solid. Finally, the elastic reflection coefficient within solid angle $\Delta\Omega$ is estimated from

$$\eta_E(\Delta\Omega)=\frac{1}{n}\sum_{k=1}^{n}\Delta I_k\ , \tag{20}$$

where n is the total number of trajectories. To obtain a reasonable accuracy, a considerable number of trajectories must be generated. This is due to the fact that the elastic backscattering probabilities are rather small, usually well below 0.1.[4,14] In the present work, the total number of trajectories for a given element and energy varied from 1×10^6 to 2×10^6. Consequently the accuracy of the elastic backscattering coefficients was better than 1%.

III. RESULTS

The Monte Carlo algorithm described above has been proven to be very reliable for the simulation of elastic electron backscattering.[24,26,27] In the present work this algorithm was applied to determine conditions of maximum backscattering efficiency from different solids. Available experimental data measured at normal incidence of the primary electron beam are, however, first compared to theory calculated in the geometry of the experiments to provide further tests on the accuracy of the algorithm.

Extensive experimental data collected at normal incidence were published by Schmid, Gaukler, and Seiler[14] and Bronshtein and Pronin.[20] Schmid, Gaukler, and Seiler[14] observed pronounced maxima in the energy dependence of the reflection coefficient within the solid angle of the retarding field analyzer, $\eta_E^{(\mathrm{RFA})}$, and indicated the shift of maxima toward higher energies with the increase of the atomic number. However, the authors explicitly stated that they cannot provide a simple argument explaining such behavior.

All the experimental energy dependences of $\eta_E^{(\mathrm{RFA})}$ published by Schmid, Gaukler, and Seiler[14] were simulated in the present work. The calculated reflection coefficient depends considerably on the IMFP.[26] It seems that the extensive tables recently published by Tanuma, Powell, and Penn[40] for the energy range 50–2000 eV are the most accurate at present, and they were exclusively used in the present work. Exemplary experimental energy dependences of the elastic reflection coefficient are compared with the results of the present calculations in Figs. 1(a)–1(e). In all cases a reasonable agreement is observed. One should pay attention to the fact that the experimental and the theoretical plots are not scaled. Thus the theory well describes not only the shape of the energy dependence but also the absolute values of the elastic reflection coefficient. The differences between experimental and theoretical energy dependences are the largest at low energies. This may be due to two reasons: (1) The theory becomes less valid at energies below 100–300 eV, depending on the atomic number of the solid, and (2) accurate experiments are more difficult to perform at low energies due to increased sensitivity of elastic backscattering to surface contaminations.

Dietzel, Meister, and Bauer[22] also observed a maximum on the energy dependence of the elastic reflection coefficient $\eta_E^{(\mathrm{RFA})}$ measured at normal incidence for amorphous silicon. Similar agreement with the present Monte Carlo calculations was observed.

Let us denote by $\eta_m^{(\mathrm{RFA})}$ and E_m the maximum value of the reflection coefficient and the corresponding energy, respectively. Figure 2 compares the experimental and theoretical values of energies E_m for a wide range of atomic numbers. Two conclusions result from this plot:

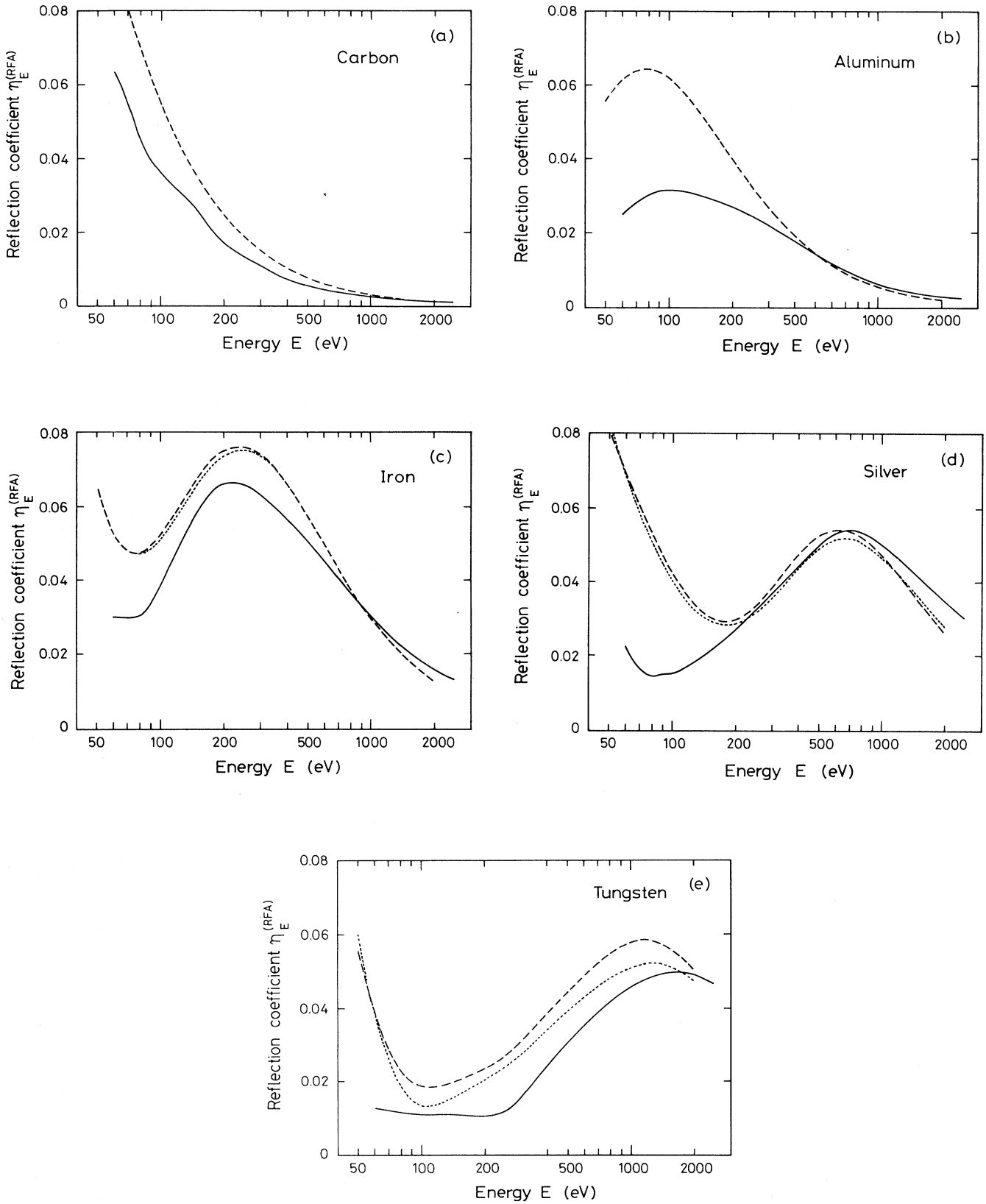

FIG. 1. Energy dependence of the reflection coefficient for the solid angle of the retarding field analyzer (RFA). Solid line: experimental dependence taken from Schmid, Gaukler, and Seiler (Ref. 14); dashed line: nonrelativistic calculations; dotted line: relativistic calculations. (a) Carbon; (b) aluminum; (c) iron; (d) silver; (e) tungsten.

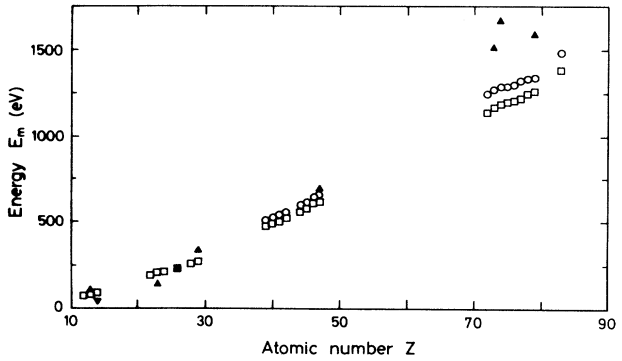

FIG. 2. Atomic number dependence of energy E_m corresponding to maximum of the elastic reflection coefficient. Triangles: values resulting from the experimental data of Schmid, Gaukler, and Seiler (Ref. 14); inversed triangle: value resulting from the experimental data of Dietzel, Meister, and Bauer (Ref. 22); squares: nonrelativistic calculations; circles: relativistic calculations.

(1) The energy corresponding to maximum intensity of elastically backscattered electrons increases monotonically with the atomic number of the target. This dependence is close to linearity.

(2) The theoretical values of E_m compare well with the experimental data.

Thus the present theory explains well the shift of E_m with the atomic number observed in available experimental data. It is then expected that the presented theoretical model is also reliable for predicting energy E_m for other materials and other acceptance angles of analyzer.

The dependence of $\eta_m^{(\mathrm{RFA})}$ on atomic number is shown in Fig. 3. The monotonic dependence on Z found for E_m (Fig. 2) is not observed for $\eta_m^{(\mathrm{RFA})}$, although again the agreement of theory with experimental values is reasonable. The considerable scatter with small variations in Z of the maximum reflection coefficients is caused by their sensitivity to parameters, in particular to the IMFP and the atomic density, which do not vary monotonically with the atomic number. The close to linear correlation

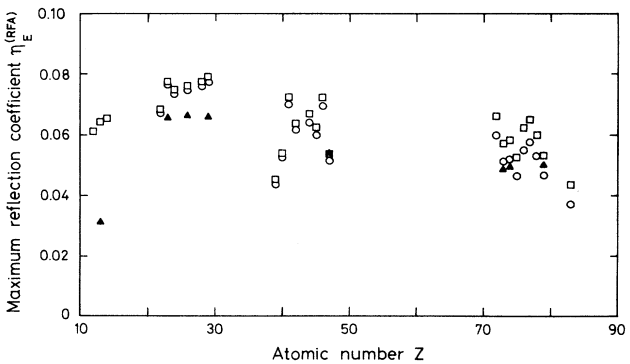

FIG. 3. Atomic number dependence of maximum of the elastic reflection coefficient $\eta_m^{(\mathrm{RFA})}$. Triangles: values resulting from the experimental data of Schmid, Gaukler, and Seiler (Ref. 14); squares: nonrelativistic calculations; circles: relativistic calculations.

between the energy E_m and the atomic number (Fig. 2) indicates that the values of E_m are influenced by the IMFP to a negligible extent, and seem to be determined mainly by the elastic scattering cross sections. Similar effects were observed by Jablonski *et al.*[26] They compared the energy dependence of the elastic backscattering intensity calculated for two different values of the IMFP. Increase of the IMFP was found to increase the backscattered intensity for all energies; however, the energy position of the maximum is not affected.

Bronshtein and Pronin[20] published energy dependences of elastic backscattering intensity measured for several elements in a direction of 25° to the surface normal. These experimental data are compared with the results of the present calculations in Figs. 4(a)–4(d). The agreement between the experiments and the theoretical calculations is very good. The experimental curves were plotted in arbitrary units. However, *the same factor was used to scale the experimental data for all elements.* This shows that theory predicts quite accurately the shape of the energy dependence of intensity and also the relative intensities for different elements.

Very extensive Monte Carlo simulations of elastic backscattering from surfaces were made in the present work to study in detail the behavior of the maximum in the energy dependence of the elastic backscattering intensity. The extent of these calculations is described below:

(1) Simulations were made at normal incidence of the primary electron beam for 27 elements, i.e., all elements for which Tanuma, Powell, and Penn[40] published recently the values of the IMFP.

(2) For each element, calculations were repeated at 30 energies logarithmically distributed in the energy range from 50 to 2000 eV. At each energy the elastic scattering cross sections were calculated and then used in the Monte Carlo simulations.

(3) For elements with atomic number up to 14 the number of generated electron trajectories was 2×10^6. The number of trajectories for elements with higher atomic numbers was 1×10^6. In effect, the statistical error of the calculated reflection coefficient decreased below 1%.

(4) The elastic backscattering intensity was calculated in 20 directions between surface normal and the plane of the surface.

(5) All the above calculations were made using the relativistic elastic scattering cross sections. Selected runs were also made for nonrelativistic cross sections.

Figure 5 shows exemplary energy dependences of the elastic backscattering intensity calculated for molybdenum at different escape angles α. One can see that theory predicts the presence of two maxima in certain directions. Both maxima shift toward higher energies with the increase of the escape angle α. For high-atomic-number elements this picture is even more complex since the number of maxima increases up to 4.

An attempt has been made to summarize positions and values of all maxima for the considered elements and geometries. At first a simple procedure was elaborated for determining the exact position of maximum from the Monte Carlo results. It is convenient to express the in-

tensity as the reflection coefficient $\Delta\eta$ within a certain small solid angle $\Delta\Omega$ divided by this solid angle:

$$I=\frac{\Delta\eta}{\Delta\Omega} .$$

A polynomial of the third degree was fitted to the points in the vicinity of the maximum in the semilogarithmic scale (see Fig. 6). From this, the position E_m of the maximum and the corresponding intensity I_m were calculated analytically from the fitted polynomial. Such calculations were repeated for numerous elements and directions α. It has been decided to plot the position of the maximum and the corresponding intensity as a function of the direction with respect to the surface normal. In this way it is possible to follow multiple maxima in the energy dependences. Plots for selected elements are shown in Figs. 7(a)–7(e).

The calculated results of E_m and I_m as a function of α for all 27 elements can be divided into five groups, corresponding to different numbers of maxima or to distinctly different intensities I_m. These groups can be defined by separate ranges of the atomic number:

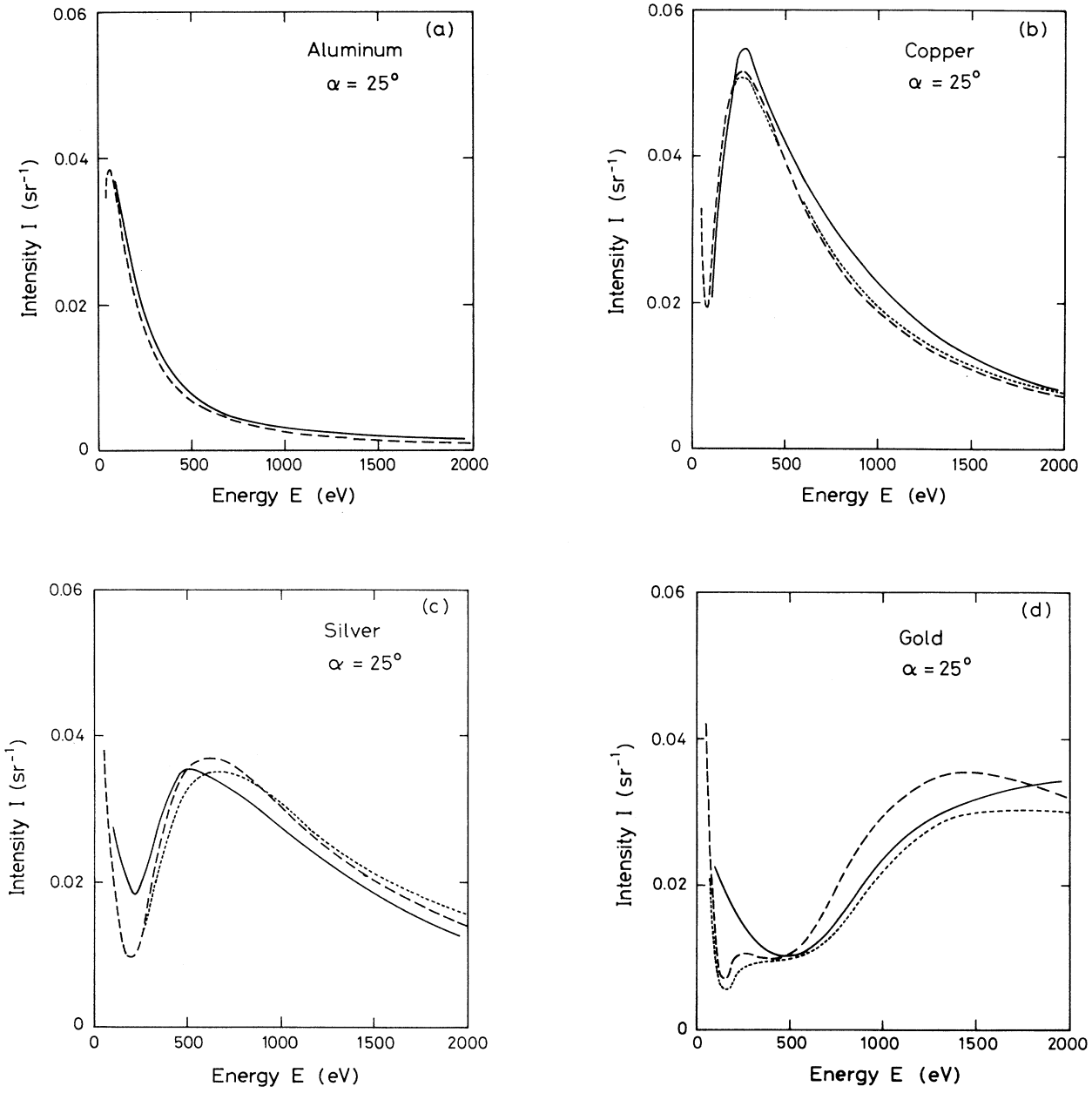

FIG. 4. Energy dependence of the elastic backscattering intensity I. Solid line: experimental dependence taken from Bronshtein and Pronin (Ref. 20); dashed line: nonrelativistic calculations; dotted line: relativistic calculations. The intensity scale refers to the calculated values. The experimental values are in arbitrary units; however *the same scaling factor was used for all elements.* (a) Aluminum; (b) copper; (c) silver; (d) gold.

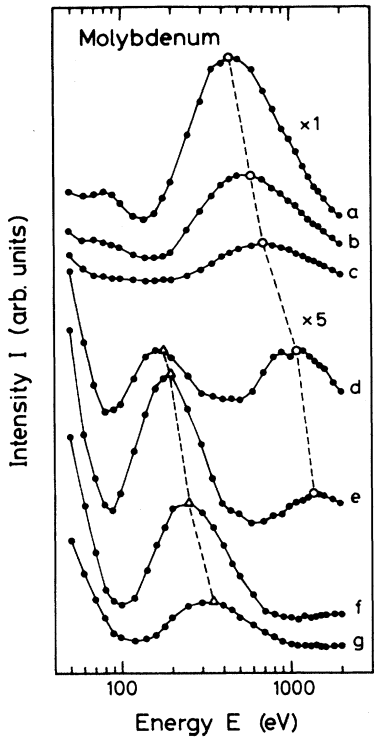

FIG. 5. Energy dependence of the elastic backscattering intensity I at different escape angles α calculated for molybdenum within the relativistic theory. (a) $\alpha=7°$; (b) $\alpha=25°$; (c) $\alpha=34°$; (d) $\alpha=43°$; (e) $\alpha=52°$; (f) $\alpha=70°$; (g) $\alpha=79°$. Note two maxima appearing at certain escape angles. Dashed line indicates the shift of the maxima positions.

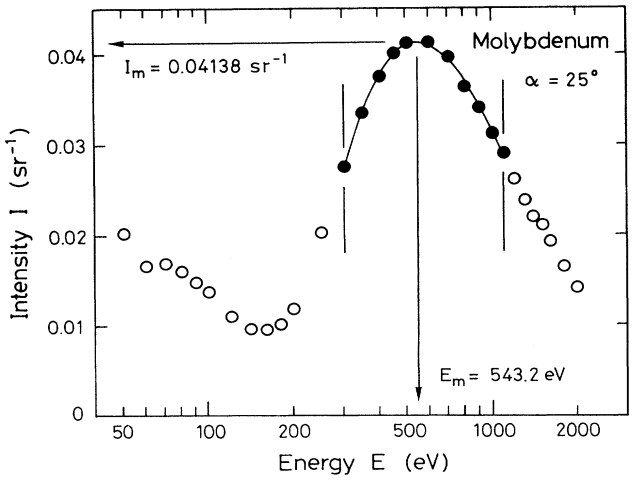

FIG. 6. Illustration of determining the maximum intensity I_m and the corresponding energy E_m by fitting the calculated values with the polynomial of the third degree.

(1) $12 \leq Z \leq 14$. One monotonically varying curve corresponding to one maximum [example shown in Fig. 7(a)].

(2) $22 \leq Z \leq 24$. One monotonically varying curve with higher intensity I_m [example shown in Fig. 7(b)].

(3) $26 \leq Z \leq 29$. Two maxima [example shown in Fig. 7(c)].

(4) $39 \leq Z \leq 47$. Two maxima with distinctly different intensity I_m [example shown in Fig. 7(d)].

(5) $72 \leq Z \leq 83$. Four maxima [example shown in Fig. 7(e)].

Differences between plots within a particular group are not very significant. One can see that more than one maximum is observed for elements with atomic number exceeding 24. As mentioned above, the theory describes particularly well the energy dependences of elastic backscattering intensity for energies exceeding 100–300 eV. Thus the maxima at higher energies (indicated by circles and solid lines) should be predicted more reliably than the low-energy maxima (triangles and dotted lines).

IV. DISCUSSION

The plots in Figs. 7(a)–7(e) may be used as preliminary aid to determine maximum intensity of elastically backscattered electrons for a given experimental geometry determined by the escape angle α. One should remember that all the results discussed refer to the normal incidence of the primary electron beam. Let us consider briefly all factors affecting the accuracy of these results.

The present calculations are made for a theoretical model assuming the random distribution of the scattering centers with density equal to the atomic density of a given solid. This is an idealized model of polycrystalline or amorphous solids, and thus the proposed theory should be applicable to such materials. This statement is well supported by the agreement with experimental data shown in Figs. 1 and 4. One can notice in Figs. 1(d), 1(e), 4(c), and 4(d) a distinct difference between energy dependence of the reflection coefficient due to relativistic and nonrelativistic calculations. This difference increases with the increase of the atomic number of the target material and is obviously due to the difference between relativistic and nonrelativistic elastic scattering cross sections. A similar observation was published recently for gold.[27] The difference cannot be ascribed to the computational errors. Care was taken to develop an accurate and stable procedure for integration of the first-order differential equations [Eqs. (10) and (12)]. This procedure made it possible to maintain the accuracy of eight decimal digits during integration. A question arises: Which algorithm, relativistic or nonrelativistic, better compares with the experimental data? This problem cannot be finally decided on the basis of the present results. However, the energy dependences of the reflection coefficient calculated in the present work from the relativistic model seem to be slightly closer to the experimental data than the dependences resulting from the nonrelativistic model [e.g., Figs. 1(e) and 4(d)]. Jablonski[27] made extensive comparisons of theoretical predictions with experimental data on the angular distribution of electrons

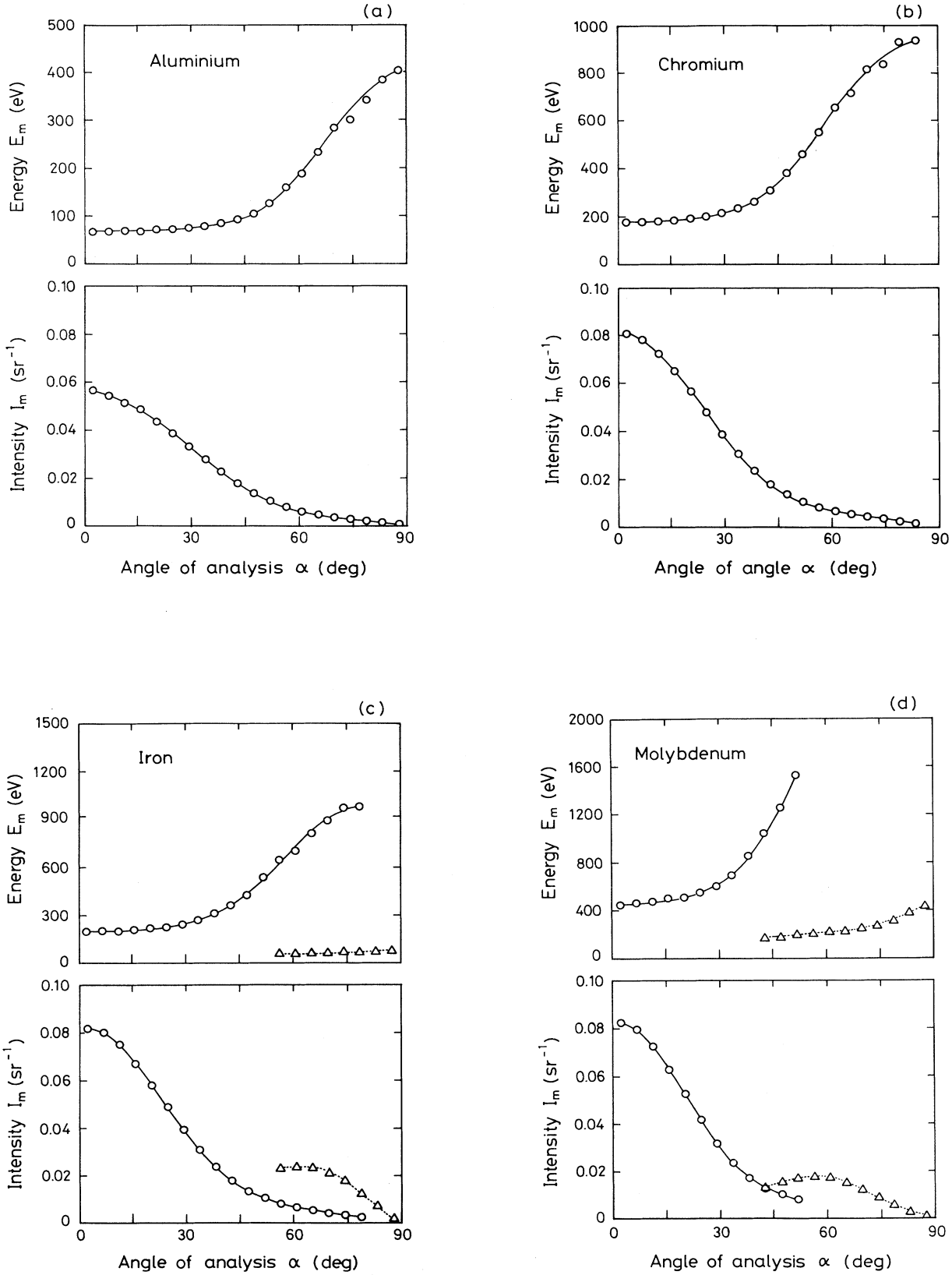

FIG. 7. Dependence of the maximum intensity I_m and the corresponding energy E_m on the escape angle α. Circles and triangles denote different maxima. The solid and dotted lines are to guide the eye through the calculated points. (a) Aluminum; (b) chromium; (c) iron; (d) molybdenum; (e) tungsten.

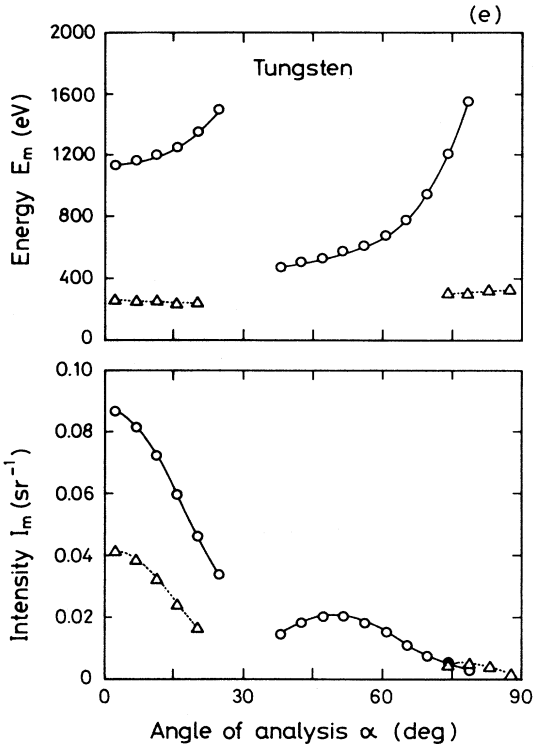

FIG. 7. (*Continued*).

elastically backscattered from gold. This analysis also favored the relativistic calculations. For this reason, it has been decided in the present work to use the relativistic algorithm for determining the behavior of the maxima in the energy dependences of elastically backscattered intensity.

Let us briefly consider the possible sources of the discrepancies between theory and experiment. Part of these discrepancies is certainly due to the simplifications of the theory describing the electron transport. As mentioned, the assumption of a two-body interaction may be less valid at low energies, where actually the largest differences are observed. Furthermore, the approximation of the scattering potentials by the potential of the isolated atom may also contribute to the errors. This problem has been analyzed recently.[27] The angular distributions of the elastically backscattered electrons and the reflection coefficient obviously depend on the potential used in the calculations. However, the corresponding deviation was found to decay with increasing energy. In the case of gold, the Thomas-Fermi-Dirac potential provided results similar to the Dirac-Hartree-Fock-Slater (DHFS) potential at energies exceeding 200–400 eV. Thus we may expect that deviations of the TFD potential from the actual potential of the scattering center do not significantly affect the results of the calculations at sufficiently high energy. The fact that the presented theory does not depend critically on the potential used explains the good agreement of the calculated parameters with the experimental observations despite the relative simplicity of the TFD potential. Similarly, the TFD potential was successfully used by other authors in calculations associated with elastic scattering of electrons.[25,41–43]

As mentioned earlier, deviations between theory and experiment at low energies may also be due to the experimental difficulties, in particular to an increased sensitivity of the elastic electron backscattering to surface contaminations.

Among the input parameters in the Monte Carlo algorithm, the values of the IMFP seem to be known with the least accuracy. Numerous data are available in the literature;[40,44–47] however, they differ considerably. One of the reasons for this scatter is the differences in definitions of the IMFP used by different authors.[48,49] In the present work all the values of the IMFP originate from one recent source,[40] which seems to be the most accurate. Thus the results of the calculations should be burdened with a similar systematic error. As shown in the present work, the inaccuracy in the values of the IMFP affects mainly the calculated maximum intensity of the backscattered electrons, while the corresponding energies seem not to be affected. For this reason, the values E_m compiled in Fig. 7 should be burdened with smaller error due to uncertainty of the IMFP than the values of I_m.

V. CONCLUSIONS

A number of experimental surface-sensitive techniques make use of elastically backscattered electrons in the energy range 50–3000 eV. In this energy range the intensity of elastically backscattered electrons usually passes a maximum. Knowledge of the position of this maximum and its value may be important to optimize such experimental techniques.

In the present work, a systematic Monte Carlo simulation, which account for multiple elastic collisions with randomly distributed scattering centers, was applied to calculate elastic backscattering intensities from surfaces of polycrystalline solids with normal incident electrons. Thus the intensity of the maximum and the corresponding energy were studied under variation of the exit angle for 27 elements in the energy range from 50 to 2000 eV. The relativistic elastic scattering cross sections were calculated assuming an electron-atom interaction potential described by the Thomas-Fermi-Dirac potential. The inelastic electron mean free path was taken from existing theoretical tabulations by Tanuma, Powell, and Penn.[40]

By comparison to available experimental data, it is found that the present theory explains well the shift of the energy position of the intensity maximum with the atomic number. In addition, not only the shape of the energy dependence but also the absolute values of the elastic reflection coefficients are predicted with reasonable accuracy. It is therefore expected that the presented theoretical prediction of the maximum is reliable also for other materials and other analyzer acceptance angles. The present data thus provide useful data for experimental techniques involving elastically backscattered electrons. Several maxima in the energy dependence of the elastic reflection coefficient are predicted in certain experimental geometries.

[1]J. Kirschner and P. Staib, Phys. Lett. **42**, 335 (1973).
[2]J. Kirschner and P. Staib, Appl. Phys. **6**, 99 (1975).
[3]J. Pawluch and L. Eckertova, Surf. Sci. **162**, 896 (1985).
[4]G. Gergely, Surf. Interface Anal. **3**, 201 (1981).
[5]G. Gergely, Vacuum **33**, 89 (1983).
[6]G. Gergely, Scanning **8**, 203 (1986).
[7]B. Gruzza, B. Achad, and C. Pariset, J. Phys. D **19**, 137 (1986).
[8]B. Gruzza and C. Pariset, J. Phys. D **22**, 717 (1989).
[9]B. Gruzza and C. Pariset, Surf. Sci. **247**, 408 (1991).
[10]C. Jardin, S. Kessas, B. Khelifa, P. Bondot, and B. Gruzza, J. Phys. D **24**, 1115 (1991).
[11]A. Jablonski, Surf. Sci. **151**, 166 (1985).
[12]W. Dolinski, S. Mróz, and M. Zagórski, Surf. Sci. **200**, 361 (1988).
[13]B. Lesiak, A. Jablonski, Z. Prussak, and P. Mrozek, Surf. Sci. **223**, 213 (1989).
[14]R. Schmid, K. H. Gaukler, and H. Seiler, in *Scanning Electron Microscopy/1983,* edited by O. Johari (SEM, Chicago, 1983), Vol. II, p. 501.
[15]O. C. Wells, Appl. Phys. Lett. **19**, 232 (1971).
[16]W. Eckstein, Z. Phys. **203**, 59 (1967).
[17]L. Loth, Z. Phys. **203**, 66 (1967).
[18]J. S. Schilling and M. B. Webb, Phys. Rev. B **2**, 1665 (1970).
[19]I. M. Bronshtein, V. P. Pronin, and V. M. Stozharov, Fiz. Tverd. Tela (Leningrad) **16**, 2107 (1974) [Sov. Phys. Solid State **16**, 1374 (1975)].
[20]I. M. Bronshtein and V. P. Pronin, Fiz. Tverd. Tela (Leningrad) **17**, 2086 (1975) [Sov. Phys. Solid State **17**, 1363 (1976)].
[21]I. M. Bronshtein and V. P. Pronin, Fiz. Tverd. Tela (Leningrad) **17**, 2502 (1975) [Sov. Phys. Solid State **17**, 1672 (1976)].
[22]W. Dietzel, G. Meister, and E. Bauer, Z. Phys. B **47**, 189 (1982).
[23]T. Oguri, H. Ishioka, H. Fukuda, and M. Irako, J. Phys. Soc. Jpn. **55**, 414 (1986).
[24]A. Jablonski, H. S. Hansen, C. Jansson, and S. Tougaard, Phys. Rev. B **45**, 3694 (1992).
[25]S. Ichimura and R. Shimizu, Surf. Sci. **112**, 386 (1981).
[26]A. Jablonski, J. Gryko, J. Kraaer, and S. Tougaard, Phys. Rev. B **39**, 61 (1989).
[27]A. Jablonski, Phys. Rev. B **43**, 7546 (1991).
[28]T.-Y. Wu and T. Ohmura, *Quantum Theory of Scattering* (Prentice-Hall, Englewood Cliffs, NJ, 1962).
[29]N. F. Mott and H. S. W. Massey, *The Theory of Atomic Collisions* (Clarendon, Oxford, 1965).
[30]F. Calogero, *Variable Phase Approach to Potential Scattering* (Academic, New York, 1967).
[31]H. Faxén and J. Holtsmark, Z. Phys. **45**, 307 (1927).
[32]A. Jablonski, Surf. Sci. **188**, 164 (1987).
[33]L. H. Thomas, J. Chem. Phys. **22**, 1758 (1954).
[34]R. A. Bonham and T. G. Strand, J. Chem. Phys. **39**, 2200 (1963).
[35]S.-R. Lin, N. Sherman, and J. K. Percus, Nucl. Phys. **45**, 492 (1963).
[36]P. J. Bunyan and J. K. Schonfelder, Proc. Phys. Soc. London **85**, 455 (1965).
[37]A. Jablonski, Surf. Interface Anal. **14**, 659 (1989).
[38]K. Murata, J. Appl. Phys. **45**, 4110 (1974).
[39]F. Salvat and J. Parellada, J. Phys. D **17**, 185 (1984).
[40]S. Tanuma, C. J. Powell, and D. R. Penn, Surf. Interface Anal. **17**, 911 (1991).
[41]S. Ichimura, M. Aratama, and R. Shimizu, J. Appl. Phys. **51**, 2853 (1980).
[42]D. Ze-jun and R. Shimizu, Surf. Interface Anal. **10**, 253 (1987).
[43]D. Liljequist, F. Salvat, R. Mayol, and J. D. Martinez, J. Appl. Phys. **65**, 2431 (1989).
[44]D. R. Penn, J. Electron Spectrosc. Relat. Phenom. **9**, 29 (1976).
[45]C. J. Tung, J. C. Ashley, and R. H. Ritchie, Surf. Sci. **81**, 427 (1979); J. C. Ashley and C. J. Tung, Surf. Interface Anal. **4**, 52 (1982).
[46]M. P. Seah and W. A. Dench, Surf. Interface Anal. **1**, 2 (1979).
[47]D. R. Penn, Phys. Rev. B **35**, 482 (1987).
[48]C. J. Powell, in *Scanning Electron Microscopy/1984,* edited by O. Johari (SEM, Chicago, 1984), Vol. IV, p. 1649.
[49]C. J. Powell, J. Electron Spectrosc. Relat. Phenom. **47**, 197 (1988).